

EFFECT OF THE pd AND dd REACTIONS ENHANCEMENT IN DEUTERIDES TiD_2 , ZrD_2 , AND Ta_2D IN THE ASTROPHYSICAL ENERGY RANGE

V. M. Bystritsky^{a,1}, *J. Huran*^b, *G. N. Dudkin*^c, *A. R. Krylov*^a,
B. A. Nechaev^c, *V. N. Padalko*^c, *F. M. Pen'kov*^d,
Yu. Zh. Tuleushev^d, *A. V. Philippov*^a, *M. Filipowicz*^e

^a Joint Institute for Nuclear Research, Dubna

^b Institute of Electrical Engineering, SAS, Bratislava

^c National Scientific Research Tomsk Polytechnic University, Tomsk, Russia

^d Institute of Nuclear Physics, Almaty, Kazakhstan

^e Faculty of Energy and Fuels, AGH University of Science and Technology, Cracow, Poland

Investigation of the pd and dd reactions in the ultralow energy (\sim keV) range is of great interest in the aspect of nuclear physics and astrophysics for developing correct models of burning and evolution of stars. This report presents compendium of experimental results obtained at the plasma pulsed Hall accelerator (TPU, Tomsk). Most of those results are new, such as: temperature dependence of the neutron yield in the $D(d, n)^3He$ reaction in ZrD_2 , Ta_2D , TiD_2 ; potentials of electron screening and respective dependence of astrophysical S factors in the dd reaction for the deuteron collision energy in the range of 3–6 keV, with ZrD_2 , Ta_2D and TiD_2 temperature in the range of 20–200°C; characteristics of the $D(p, \gamma)^3He$ reaction in the ultralow collision proton–deuterons energy range of 4–13 keV in ZrD_2 , Ta_2D , and TiD_2 ; observation of the neutron yield enhancement in the $D(d, n)^3He$ reaction at the ultralow deuteron collision energy due to channeling of deuterons in microscopic TiD_2 with a face-centered cubic lattice type $TiD_{1.73}$, oriented in the [100] direction.

The report includes discussion and comparison of the collected experimental results with the global data and calculations.

Представлена совокупность экспериментальных результатов по изучению pd - и dd -реакций, протекающих в дейтеридах TiD_2 , ZrD_2 и Ta_2D в области ультранизких энергий, полученных с использованием плазменного импульсного ускорителя Холла (ТПУ, Томск). Большинство из этих результатов являются пионерскими: исследованы температурные зависимости выходов нейтронов из реакции $D(d, n)^3He$, протекающей в дейтеридах титана, циркония и тантала; измерены потенциалы электронного экранирования реакции, а также зависимости астрофизических S -факторов от энергии столкновения дейтронов в интервале 3–6 кэВ в устойчивых фазовых состояниях ZrD_2 , Ta_2D и TiD_2 в диапазоне температур 20–200°C; измерены характеристики реакции $D(p, \gamma)^3He$, протекающей в дейтеридах титана, циркония и тантала в области ультранизких энергий столкновения протонов с дейтронами 4–13 кэВ; исследован эффект увеличения выхода нейтронов в $D(d, n)^3He$ -реакции при ультранизких энергиях за счет каналирования дейтронов

¹E-mail: bystvm@jinr.ru

в микрокристаллах дейтерида титана с кубической гранцентрированной решеткой типа $\text{TiD}_{1,73}$, ориентированных в направлении [100].

Приводится обсуждение и сравнение полученных экспериментальных результатов с мировыми данными и расчетами.

PACS: 25.45.-z; 25.10.+s; 95.30.Cq

INTRODUCTION

Study of reactions between light nuclei in ultralow energy region (\sim keV)

$$dd \rightarrow {}^3\text{He}(0.8 \text{ MeV}) + n(2.5 \text{ MeV}), \quad (1a)$$

$$dd \rightarrow p(3.0 \text{ MeV}) + t(1.03 \text{ MeV}), \quad (1b)$$

$$pd \rightarrow {}^3\text{He} + \gamma(5.5 \text{ MeV}), \quad (2)$$

$$d^3\text{He} \rightarrow p(14.7 \text{ MeV}) + {}^4\text{He}(3.7 \text{ MeV}), \quad (3)$$

$$d^3\text{He} \rightarrow {}^5\text{Li} + \gamma(16.4 \text{ MeV}), \quad (4)$$

$$d^6\text{Li} \rightarrow 2\alpha(22.4 \text{ MeV}) \quad (5)$$

is of a great interest due to the possibility of: verification of fundamental symmetries in strong interaction (charge and isotopic invariance of nuclear forces) [1, 2]; acquisition of information on contribution and structure of exchange meson currents [3, 4], whose contribution into interaction in the ultralow energy region becomes significant (e.g., in case of radiative capture of protons by deuterons and tritons: $p + d \rightarrow {}^3\text{He} + \gamma$; $p + t \rightarrow {}^4\text{He} + \gamma$); acquisition of information for microscopic description of nucleon–nucleon interaction; testing of theoretical articles, dedicated to three-body tasks solution based on modern representation of nucleon–nucleon interaction potential within the bounds of realistic two-body, two-body plus three-body forces [5]. Concerning astrophysics, there is a need for the reliable experimental information on parameters of all general processes, included in hydrogen and carbon cycles, that occur in the stars with ultralow energy of nuclear interaction [6–8]. It is assumed in the modern star models that at high level of the star matter density reached in the process of the star evolution, the rate of nuclear reactions increases due to the screening of positively charged nuclei by negatively charged electrons (electron screening (ES) results in the effective decrease of the Coulomb barrier and thus in the increase of the nuclear reaction rate [9–11]).

In the recent time, there has been an increase in the interest in the study of the mechanism of reactions between light nuclei (pd , dd) in metals saturated by hydrogen isotopes in the range of ultralow energies [12–18]. The obtained results of the studied reactions $\text{D}(d, n){}^3\text{He}$ and $\text{D}(d, p)t$ in the last decade [12–18] show the existence of an enhancement effect in the reaction of the dd synthesis in deuteride metals, resulting from the presence of electron screening of deuterium nuclei. To verify the existence of this effect, we have conducted experiments with beams of deuterons accelerated by a pulse Hall accelerator and using targets with deuterides of titanium, zirconium, and tantalum [19–21]. As a result, the electron screening potential of deuterons interacting in the deuterides of metals has been obtained. Notwithstanding the above, as an alternative to the electron screening mechanism, the presence of a channeling mechanism of the beam’s deuterons during the dd reaction in TiD_2 was considered [22–24].

There is still no clear conclusion concerning the contribution of these two mechanisms into the effect of the dd -reaction enhancement. To obtain an answer to this question, it is necessary to perform a study of the dd reaction in varied metallic targets and for varied levels of saturation by deuterium. An analogous research has been performed in order to study the enhancement effect in the $D(p, \gamma)^3\text{He}$, $(H(d, \gamma)^3\text{He})$ reactions [25–29], which occur in metallic targets saturated by deuterium (reaction (2)) or by hydrogen (reaction $(H(d, \gamma)^3\text{He})$).

From the standpoint of nuclear physics, it is particularly interesting to study the pd reaction in the region of ultralow proton–deuteron collision energies as a mirror reaction with respect to the reaction of radiative neutron capture by a deuteron [3, 4].

The purpose of this work is the presentation of the fresh results obtained recently by us and devoted to the investigation of the pd and dd reactions undergoing in different substances in the ultralow energy region.

1. MEASUREMENT METHOD

The experimental determination of the astrophysical S factors and electron screening potentials U_e for the pd and dd reactions is based on the measuring of the yield of 5.5 MeV gamma quanta from the pd reaction N_{γ}^{exp} and 2.5 MeV neutron from the dd reaction N_n^{exp} using parameterization [19–21, 25–29]:

$$N_{\gamma(n)}^{\text{exp}} = N_{p(d)} \varepsilon_{\gamma(n)} \int_0^{\infty} F_{p(d)}(E) dE \int_0^E \frac{S_{pd(dd)}^b(E')}{(E' + U_e)} \times \\ \times \exp(-2\pi\eta(E' + U_e)) n_d(x) \left(\frac{dE}{dx}\right)^{-1} dE', \quad (6)$$

$$\sigma_{pd(dd)}^b(E) = \frac{S_{pd(dd)}^b(E)}{E} \exp(-2\pi\eta(E)), \quad 2\pi\eta = 31.29 Z_1 Z_2 \left(\frac{\mu}{E}\right)^{1/2}, \quad (7)$$

$$\sigma_{pd(dd)}^{\text{scr}}(E) = \frac{S_{pd(dd)}^b(E)}{E + U_e} \exp(-2\pi\eta(E + U_e)) = \sigma_{pd(dd)}^b f_{pd(dd)}, \quad (8)$$

$$S_{pd(dd)}^{\text{scr}}(E) = S_{pd(dd)}^b f_{pd(dd)}, \quad (9)$$

$$f_{pd(dd)} = \frac{E}{E + U_e} \exp(-2\pi\eta(E + U_e) + 2\pi\eta(E)), \quad (10)$$

$$f_{pd(dd)} \approx \exp\left(\pi\eta \frac{U_e}{E}\right), \quad \text{at } U_e \ll E, \quad (11)$$

$$E_{\text{col}} = \int_0^{\infty} E P_{pd(dd)}(E) dE, \quad (12)$$

$$\overline{S_{pd(dd)}^{\text{scr}}(E)} = \int_0^{\infty} S_{pd(dd)}^{\text{scr}}(E) P_{pd(dd)}(E) dE = S_{pd(dd)}^{\text{scr}}(\bar{E}) = S_{pd(dd)}^{\text{scr}}(E_{\text{col}}) =$$

$$= \frac{N_{\gamma(n)}^{\text{exp}}}{N_{p(d)} \varepsilon_{\gamma(n)} \int_0^{\infty} F_{p(d)}(E) dE \int_0^{\infty} \frac{e^{-2\pi\eta} n_d(x)}{E'(E, x)} dx}, \quad (13)$$

$$P_{pd(dd)}(E) = \frac{e^{-2\pi\eta} D(E) \int_E^{\infty} n_d(x(E, E')) F_{p(d)}(E') dE'}{\int_0^{\infty} e^{-2\pi\eta(E+U_e)} D(E) \int_E^{\infty} n_d(x(E, E')) F_{p(d)}(E') dE'}}, \quad (14)$$

$$D(E) = -\frac{1}{E} \frac{dx}{dE}, \quad (15)$$

where $S_{pd(dd)}^b$ is the astrophysical S factor for the $pd(dd)$ reaction that assumes interaction of “bare” protons (deuterons) with deuterons (protons); $\sigma_{pd(dd)}^b$ is the cross section of the $pd(dd)$ reaction that assumes interaction of “bare” protons (deuterons) with deuterons (protons); $\sigma_{pd(dd)}^{\text{scr}}$ is the cross section of the $pd(dd)$ reaction taking into account the electron screening (ES) of nuclear charges of interacting particles in the entrance channel of reaction; μ is the reduced mass of interacting particles in the entrance channel of the reaction in a.m.u.; η is the Sommerfeld parameter; E is the center-of-mass proton–deuteron (deuteron–deuteron) collision energy; $S_{pd(dd)}^{\text{scr}}(E)$ is the astrophysical S factor for the $pd(dd)$ reaction taking into account the electron screening (ES); $N_{\gamma(n)}^{\text{exp}}$ is the total number of recorded gamma rays (neutrons) formed in the $pd(dd)$ reaction; dE/dx is the specific proton (deuteron) energy loss in the target; $n_d(x)$ is the target deuteron density at depth x ; $F_{p(d)}(E)$ is the energy distribution function for the incident protons (deuterons) with average energy $E_p(E_d)$; $\varepsilon_{\gamma(n)}$ is the detection efficiency for the gamma rays (neutrons) from the pd and dd reactions, respectively; $E'(E, x)$ is the proton–deuteron (deuteron–deuteron) collision energy in the c.m.s.; $N_{p(d)}$ is the number of protons (deuterons) arriving at the target; $P_{pd(dd)}(E)$ is the distribution function for the probability of the proton–deuteron (deuteron–deuteron) collision with subsequent recording of the gamma ray (neutron) yield from the $pd(dd)$ reaction for the c.m.s. energy E , normalized to unity; E_{col} is the proton–deuteron (deuteron–proton) collision energy averaged over the distribution function $P(E)$; f is the enhancement factor of the $pd(dd)$ reaction. At deep subbarrier energies, when the function $P(E)$ is a narrow peak, the expression for the gamma ray (neutron) yield from the $pd(dd)$ reaction $N_{\gamma(n)}$ can be written in a simple form in terms of the effective reaction cross section $\tilde{\sigma}_{pd(dd)}(E_{\text{col}})$ [30].

Calculated gamma quanta (neutron) yield from the $pd(dd)$ reaction is

$$N_{\gamma(n)}^{\text{exp}} = N_{p(d)} \varepsilon_{\gamma(n)} n_t \tilde{\sigma}_{pd(dd)}(E_m) l_{\text{eff}}(E_m) K_{\text{eff}}(E_m), \quad (16)$$

where l_{eff} — effective range of protons (deuterons) in the target; $K_{\text{eff}}(E_m)$ — fraction of the initial proton (deuteron) flux; n_t — target deuteron density; E_m — energy of the $pd(dd)$ collisions at maximum of the function $P_{pd(dd)}(E)$.

The effective cross section for the $pd(dd)$ reaction is defined as

$$\tilde{\sigma}_{pd(dd)}(E) = \frac{N_{\gamma(n)}^{\text{exp}}}{N_{p(d)} \varepsilon_{\gamma(n)} n_t l_{\text{eff}}(E_m) K(E_m)} \quad (17)$$

at the assumption that $U_e = 0$.

2. EXPERIMENTAL SETUP

The High-Current Hall Accelerator. Detection Systems. Targets. The $D(d, n)^3\text{He}$ reaction in the deuterated metals Ti, Zr, and Ta was experimentally studied using the plasma high-current Hall ion accelerator [22, 31–35] at the National Scientific Research Tomsk Polytechnic University (Tomsk, Russia).

The experimental setup (Fig. 1) comprised the plasma pulsed Hall accelerator (PHA) with closed electron current that allowed acceleration of H^+ , D^+ , and $^3\text{He}^+$ plasma ions in the energy range of 2–15 keV; scintillation detection systems to detect 2.5 MeV neutrons from the dd reaction and to detect 5.5 MeV gamma quanta from the pd reaction; three types of solid targets from deuterides of zirconium, titanium, and tantalum with a system of their warming within the range of 20 to 300°C; diagnostics equipment to monitor parameters of the deuteron (proton) beam incident on the target; and the system for monitoring the state of the target in the course of measurements.

A distinctive feature of the acceleration process in the Hall accelerator (HA) designed and built by us is conservation of quasineutrality of the accelerating ion layer due to sharply limited transverse mobility of magnetized electrons in the magnetic field [36]. Under these conditions, ion current density limitations by the space charge are removed and the limiting values of the ion current are governed by induction of the external magnetic field. This method for production of intensive ion beams is characterized by stability of the acceleration process, because the necessary level and zero lag of ion emission are provided by the external induction plasma source with pulsed gas bleeding. The design of the PHA provides the possibility of measuring parameters of the ion flow incident on the target (including energy distribution of ions) during the experiments [34, 35]. The main characteristics and advantages

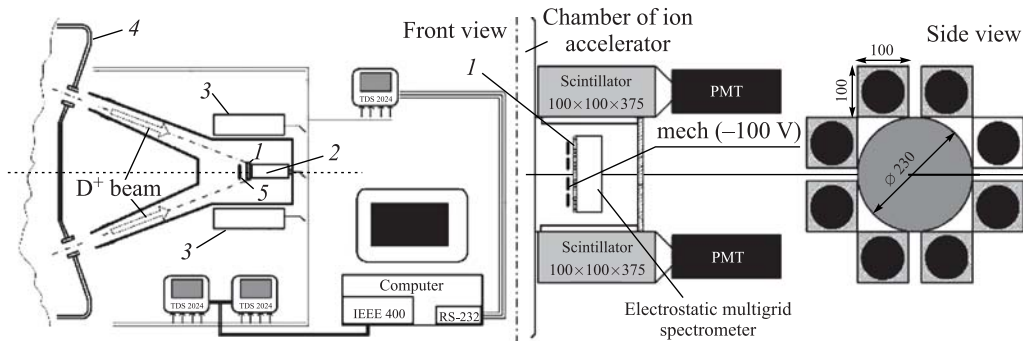


Fig. 1. Experimental setup: 1 — deuterium target; 2 — electrostatic multigrad spectrometer; 3 — plastic scintillation detectors; 4 — PHA; 5 — mesh

of the HA are the following: the plasma density is $(1-2) \cdot 10^{13} \text{ cm}^{-3}$, which corresponds to the ion saturation current $\sim 1-3 \text{ A/cm}^2$; electrode less inductive discharge in the gas provides a low level of impurities; the HA provides control in a wide range of plasma parameters with respective ion current density up to $\leq 1 \text{ A/cm}^2$; the type of the filling gas could be easily changed for generating plasma of different ion species. The targets were shaped as discs 97 mm in diameter and 2 mm thick, made of stainless steel with surface layers of Zr, Ti, and Ta deuterides of average thickness 1.2–1.5 μm deposited by reactive direct current (DC) magnetron sputtering (ALCATEL SCM650) of zirconium, titanium, and tantalum in the deuterium environment. The ultimate vacuum was less than $5 \cdot 10^{-7}$ Torr with liquid nitrogen shielding. The discharge gas was a mixture of D_2 and Ar (D_2/Ar ratio was 1:1) at the total pressure of $1.5 \cdot 10^{-2}$ Torr. The duration of the pulse of the accelerated deuteron flow generated by the Hall ion source was $\sim 10 \mu\text{s}$, the pulse repetition rate was $\sim 7 \cdot 10^{-2}$ Hz, and the integral number of deuterons in the pulse was $\sim 5 \times 10^{14}$. To determine the actual flow of the accelerated deuterons (protons) which hit the target, it is necessary to have information about the secondary electron emission from the target under the action of deuterons (protons) and neutrals formed via charge exchange of $\text{D}^+(\text{H}^+)$ ions on the residual gas in the measuring chamber of the accelerator during their transport from the PHA to the target. To suppress the emission of electrons from the target, a mesh with transparency of 93% was placed in front of the target at the distance of 1 cm and held at the potential $U_m = -100 \text{ V}$. We developed methods for measuring the coefficient of secondary electron emission and determining the total number of accelerated particles (ions and neutrals) incident on the target. In addition to these measurements, the knowledge of the composition of accelerated particles is necessary for correct interpretation of the experimental data. These measurements were carried out in experiments with the time-of-flight technique. In those experiments, a number of important parameters of the accelerated flow of particles impinging on the target were measured: the efficiency of transporting the flow of accelerated particles from the exit of the PHA to the location of the target (base $\sim 105 \text{ mm}$) in the angular span of $0-20^\circ$; the energy distribution function of the deuterons (protons) in the flow [22, 35, 37]. The experimental results indicate that the fraction of the molecular D_2^+ (H_2^+) ions in the accelerated flow is negligible ($\leq 1\%$), while the neutrals produced in the charge exchange on the residual gas in the measuring chamber of the accelerator during their transport to the target make up 10–15%, depending on the experimental conditions (the composition of the plasma source in the PHA, the partial pressure of the residual gas in the measuring chamber of the accelerator, where the ZrD_2 , TiD_2 , and Ta_2D targets were located). The DC at the exit of the PHA was measured using the Rogowski coil with a passive RC integrator. The current density distribution of the ions incident on the surface of the deuterium (hydrogen) target was measured by a linear set of the collimated Faraday cups placed along the target radius. This diagnostics provided information in each pulse of the PHA on the radial distribution of the DC density over the target surface. The area of the $\text{D}^+(\text{H}^+)$ beam cross section in the target plane was $\sim 73.9 \text{ cm}^2$. The energy distribution of the $\text{D}^+(\text{H}^+)$ ions incident on the target was measured with the multigrad electrostatic energy spectrometer located behind the target in line with the ion flow [37]. Figure 2 illustrates the integral and differential energy spectra of the deuterons which hit the ZrD_2 target in the experiment on the study of the dd reaction. The energy spread of the D^+ beam in the energy range of 4–15 keV amounted to 14–16%.

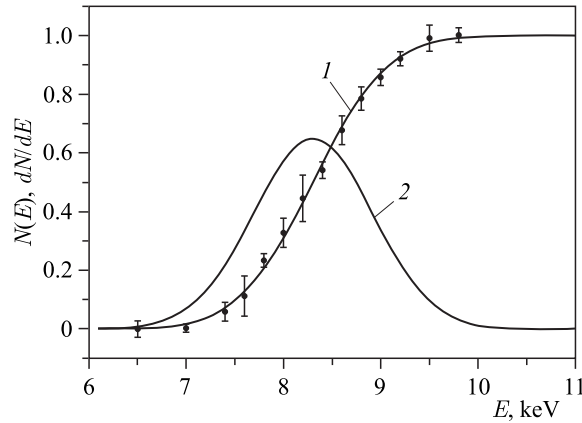


Fig. 2. Energy spectra of deuterons incident on the target: 1 — integral spectrum; 2 — differential spectrum

Neutrons with energy of 2.5 MeV from the $D(d, n)^3\text{He}$ reaction were detected by eight counters based on plastic scintillators, $100 \times 100 \times 375$ mm in size, placed around the measuring chamber of the accelerator (see Fig. 1). The neutron detection efficiency was calculated by the Monte Carlo simulation using the results of calibration of the detectors with the standard sources of neutrons (^{252}Cf , ^{239}Pu) and gamma rays (^{137}Cs , ^{60}Co , ^{228}Th). The relative neutron detection efficiency at the experimental energy threshold of recoil proton detection (160 ± 6) keV was found to be 0.230 ± 0.013 . The given estimate of the efficiency is a summation of the statistical deviation: the geometry error in defining the distance and the location of the neutron detectors with respect to the target; the error in the measurement of the radial distribution of the impinging beam deuterons over the target; the error in defining the threshold amplitude of the neutron detection system; the errors in the cross-section values of the interactions of neutrons with the energy of 2.5 MeV with different substances located between the target and the neutron detectors, and also with the plastic scintillator.

Gamma rays with the energy $E_\gamma = 5.5$ MeV from the pd reaction were recorded by eight NaI(Tl)-based detectors ($100 \times 100 \times 400$ mm) placed around the target. The detection efficiency for gamma rays from reaction (2) was determined by the Monte Carlo method. At the detector energy threshold of 3 MeV, it was $\varepsilon_\gamma = 0.300 \pm 0.006$. This threshold was chosen to suppress the background caused by neutrons from the dd fusion reaction $d + d \rightarrow ^3\text{He} + n$ (2.5 MeV), which is quite probable to occur due to the deuterium impurity of the proton beam (the relative concentration of deuterium in hydrogen is $\sim 10^{-4}$ and the dd -reaction cross section in the energy region under study is three to four orders of magnitude larger than the pd -reaction cross section).

The background from cosmic radiation and natural radioactivity was continuously monitored during the experiments. To this end, in the intervals between the working pulses of the accelerator, background events were recorded for a period of time as long as $10 \mu\text{s}$, which was equal to the duration of those pulses, during which the accelerated proton beam was impinging on the TiD_2 (ZrD_2 , Ta_2D) target. The energy resolution average over all eight gamma detectors, measured for the 2.5 MeV total absorption peak line of the ^{60}Co source, was 4.3%.

The in-depth distributions of the concentrations of the base elements and impurities in the targets of zirconium, titanium, and tantalum deuterides were measured by the Elastic Recoil Detection (ERD) and Rutherford Backscattering Spectrometry (RBS) methods using the helium ion beam with the energy of 2.297 MeV [38–40] and by the method of level-by-level analysis of ZrD_2 , TiD_2 , and Ta_2D targets using the Auger electron spectroscopy [41].

3. EXPERIMENTAL RESULTS

3.1. The dd Experiment. Table 1 presents the compilation of the electronic screening potentials (ESP) values measured before starting our experiments.

Table 1. Electron screening potentials $U_e(\text{ZrD}_2)$, $U_e(\text{TiD}_2)$, and $U_e(\text{Ta}_2\text{D})$

Target	Temperature, °C	Stoichiometry	Experimental U_e , eV	Theoretical U_e , eV
ZrD	20	$\text{ZrD}_{1.1}$	≤ 40 [42]	112 [13]
	200	$\text{ZrD}_{0.13}$	205 ± 70 [14]	
	20	ZrD_2	297 ± 8 [13]	
	20	ZrD_2	319 ± 3 [16]	
TiD	–88	$\text{TiD}_{3.76}$	66 ± 15 [12]	100 [13]
	20	$\text{TiD}_{1.3}$	≤ 30 [42]	
	50	$\text{TiD}_{1.1}$	≤ 50 [14]	
	100	$\text{TiD}_{0.26}$	250 ± 40 [14]	
	150	$\text{TiD}_{0.23}$	295 ± 40 [14]	
TaD	20	$\text{TaD}_{0.13}$	340 ± 14 [43]	136 [12]
	20	TaD	322 ± 15 [44]	
	20	TaD	302 ± 13 [45]	
	–10	$\text{TaD}_{0.13}$	309 ± 12 [46]	
	20	$\text{TaD}_{0.13}$	270 ± 30 [42]	

To clarify the nature of the discrepancy between the results of the experiments [12–14, 16, 42–46] (see Table 1) on measurement of the ES potentials for reaction (1b) in TiD_2 and ZrD_2 , we experimentally studied the $\text{D}(d, n)^3\text{He}$ reaction in the ultralow deuterons energy region (7–12 keV) using the TiD_2 and ZrD_2 targets in the temperature range of 20–200°C and the plasma pulsed Hall accelerator [20]. The replacement of the $\text{D}(d, p)t$ reaction with $\text{D}(d, n)^3\text{He}$ (1a) is well grounded according to [47, 48], the ratio of cross sections in channels (1a) and (1b) of the dd reaction in the ultralow region of collision energy is near unit within the measurement errors.

In addition to the experiments on measurement of $U_e(\text{TiD}_2)$ and $U_e(\text{ZrD}_2)$, we measured the electron screening potential for the dd reaction in the deuterated tantalum target at the temperature of 60°C [21].

We have measured the dependence of the neutron yields from the $\text{D}(d, n)^3\text{He}$ reaction on the average deuteron collision energy \bar{E} in the range of 3.3–5.4 keV using the ZrD_2 and TiD_2 targets in the temperature range of 20–200°C [20]. By way of example, Fig. 3 shows

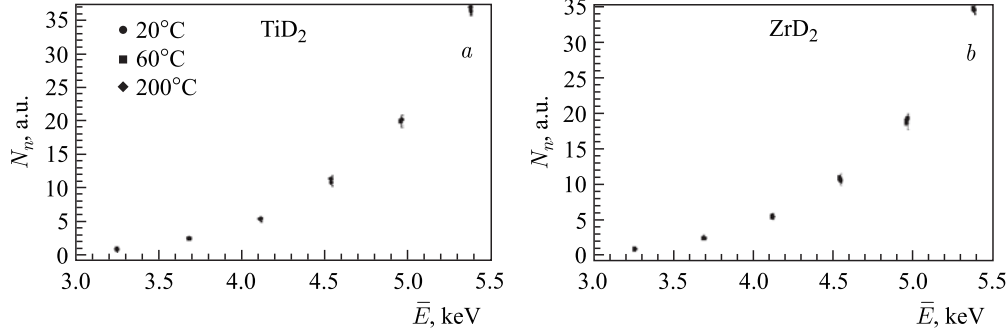


Fig. 3. Neutron yields as a function of the average deuteron collision energy at the temperatures 20, 60, and 200°C: a) TiD_2 target; b) ZrD_2 target

dependences of the neutron yields from the dd reaction on the deuteron collision energy measured in the TiD_2 and ZrD_2 targets at the temperatures 20, 60, and 200°C [20].

As is evident, the experimental results shown in Fig.3 indicate within the statistical experimental errors that the neutron yield from the dd reaction in titanium and zirconium deuterides does not depend on the temperature in the range of average deuteron collision energies from 3.3 to 5.4 keV. Considering Eq. (13), the obtained results allow the conclusion that the values of the astrophysical $S_{dd}(E)$ factors corresponding to the same average deuteron collision energies in the range of 3.3–5.4 keV do not depend on the temperature of titanium and zirconium deuterides. Thus, according to (9), the dd -reaction enhancement factor f_{dd} is also independent of the TiD_2 and ZrD_2 temperature, and so is (according to (10)) the ESP. Figure 4 shows dependence of the astrophysical S_{dd} factor on the average deuteron collision energy at the temperatures 20, 60, and 200°C for the TiD_2 and ZrD_2 targets and the ESPs for the dd reaction obtained by fitting the experimentally-measured neutron yields for the dd reaction by expression (6) using Eqs.(9) and (10), and taking into account the equation for calculation of the astrophysical factor for interaction of bare deuterons $S_b(E)$ [47]. The values of $S_b(E)$ are found from the R -matrix cross sections for the $D(d, n)^3He$ reaction by Eq. (7), using the approximation by the polynomial [47]:

$$S_b(E) = A_1 + E(A_2 + E(A_3 + E(A_4 + EA_5))), \quad (18)$$

where A_1, \dots, A_5 are parameters.

The values of electron screening potentials for the dd reaction undergoing in the ZrD_2 and TiD_2 targets at room temperature (20°C) and in the target from $TaD_{0.5}$ at $T = 60^\circ C$ are the following:

$$\begin{aligned} U_e(ZrD_2) &= (205 \pm 35) \text{ eV}, \\ U_e(TiD_2) &= (125 \pm 34) \text{ eV}, \\ U_e(TaD_{0.5}) &= (313 \pm 58) \text{ eV}. \end{aligned}$$

As to comparison of our results from the experiments on the dd reactions in the ZrD_2 and TiD_2 targets with other published experimental data (ZrD_2 [13, 16, 42]; TiD_2 [12, 14, 42]), there is a significant difference, the nature of which is still unclear. Some differences in the experiments on determination of potential electron screening energy for the dd reaction should

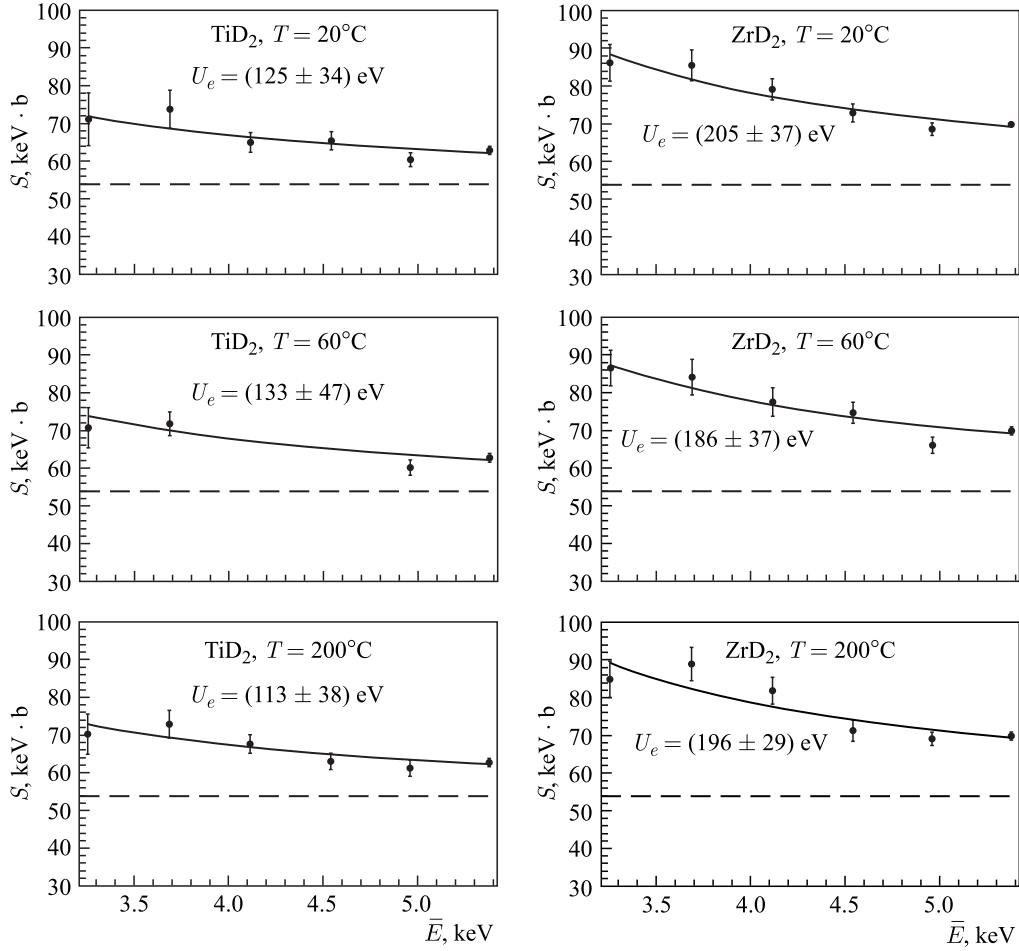


Fig. 4. Dependence of the experimental value for astrophysical S factors on the average deuteron collision energies in the c.m.s. at the target temperatures 20, 60, and 200°C. The dashed line is the calculated S -factor dependences for the dd reaction in the case of interaction of bare deuterons. Solid curves are the calculated dependence of the S factors for the dd reaction on the deuteron collision energy at the target temperatures 20, 60, and 200°C obtained with the corresponding ESPs U_e (shown directly in the plots)

be noted. We prepared the target for our experiments with predetermined stoichiometry by magnetron sputtering of zirconium and titanium in the ambient atmosphere of deuterium, in contrast to other laboratories, where the titanium and zirconium targets were implanted by a deuterium beam. One important circumstance should be mentioned. The value of the electronic screening potential averaged over the temperature interval of 20–200°C measured by us for the dd reaction in zirconium deuteride is 1.6 times higher than the corresponding value for titanium deuteride. An important result of this work is the conclusion that the ESP does not depend on temperature in the interval of 20–200°C. As regards the comparison of the results from this experiment on measurement of the ESP with the results of calculations,

there is quite good agreement for TiD_2 and a difference of about a factor of 1.6 for ZrD_2 . The nature of this disagreement is not clear yet.

To elucidate the reasons for the existing discrepancies between the values of $U_e(\text{ZrD}_2)$ and $U_e(\text{TiD}_2)$ obtained by us and the corresponding values published in other works (ZrD_2 [13, 16, 42]; TiD_2 [12, 14, 42]), it is necessary to study thoroughly the *dd*-reaction mechanisms in a variety of target materials and wide ranges of temperature and collision energy. In this regard, we plan to continue studying the $\text{D}(d, n)^3\text{He}$ and $\text{D}(d, p)t$ reactions for determining the astrophysical S_{dd} factors and electron screening energies of interacting deuterons, using the PHA and a wide range of targets made of dielectrics and metals saturated with deuterium.

Situation with the study of the *dd* reaction in $\text{TaD}_{0.5}$ at the target temperature of 60°C is the following [21]. The measured value of $U_e(\text{TaD}_{0.5})$ agrees in the range of statistical errors with the results of [13, 44–46] obtained at the temperature of 20°C , as well as with the results obtained at $T = 10^\circ\text{C}$ [46]. Note that total errors of the measured values of $U_e(\text{TiD}_2)$, $U_e(\text{ZrD}_2)$, and $U_e(\text{TaD}_{0.5})$ include both statistical and systematic ones.

Summing up, we have the following:

- ESP does not depend on temperature in the interval of $20\text{--}200^\circ\text{C}$.
- ESP averaged on temperature interval of $20\text{--}200^\circ\text{C}$ measured in zirconium deuteride is 1.6 times higher than the corresponding value for titanium deuteride.
- Measured value of ESP for TiD_2 is in quite good agreement with calculation.
- Measured value of ESP for the ZrD_2 deuteride is not agreed of 1.6 factor in comparison with calculation.
- To elucidate the reasons for the existing discrepancies between the values of $U_e(\text{ZrD}_2)$ and $U_e(\text{TiD}_2)$ existing in the literature, it is necessary to study the *dd*-reaction mechanisms in a variety of target materials and wide ranges of temperature and collision energy.
- Found value of $U_e(\text{TaD}_{0.5})$ is in agreement with the values of the corresponding quantity in the literature.

3.2. Channeling Enhancement Effect of *dd* Nuclear Reactions. In recent years, as noted in Subsec. 3.1, in a number of experiments [12–21, 42–46], an increase of the (1a) and (1b) reaction cross sections at the deuteron ultralow collision energies below 10 keV has been observed. This phenomenon is very similar to an increase in the nuclear reaction rate in the central region of the Sun caused by the Debye screening of the nuclear Coulomb potential [9, 49] and to the effect of screening of interacting nuclei by atomic electrons [50]. Within the screening model, the nuclear reaction cross section $\sigma(E)$ for screened nuclei is determined by reaction cross section for bare nuclei $\sigma_b(E)$ with energy shifted by the value of the screening potential U_e [9]: $\sigma(E) = \sigma_b(E + U_e)$. Considering weak energy dependence of the astrophysical S factor, this increase expressed by the f_{dd} factor is determined by the Coulomb penetration factor [9]: $\sigma(E) = \sigma_b(E + U_e) = \sigma_b(E)f(E)$, $f(E)_{dd} \approx \exp(\pi\eta(E)U_e/E)$, which can be considerably large in the deep-subbarrier energy region ($2\pi\eta(E) \gg 1$). Naturally, this enhancement also applies to the S factor: $S_{dd}(E) = S_b(E)f$. The upper scale boundary of the screening potential 40.8 eV is dictated by the adiabatic limit [9], i.e., by the difference of the helium ion and hydrogen atoms binding energies. It is easy to make sure that the Coulomb interaction of the incident deuteron with the electron and deuterium nucleus average over the hydrogen atom wave functions determines the screening potential $U_e = 27.2$ eV. This value is very close to the experimental screening potential value (27 ± 5) eV obtained for the $\text{D}(d, p)t$ reaction in a gas target [48]. The screening within the Thomas–Fermi model [50] in the theory of metals yields ion screening potentials within the range from 17 to 30 eV that

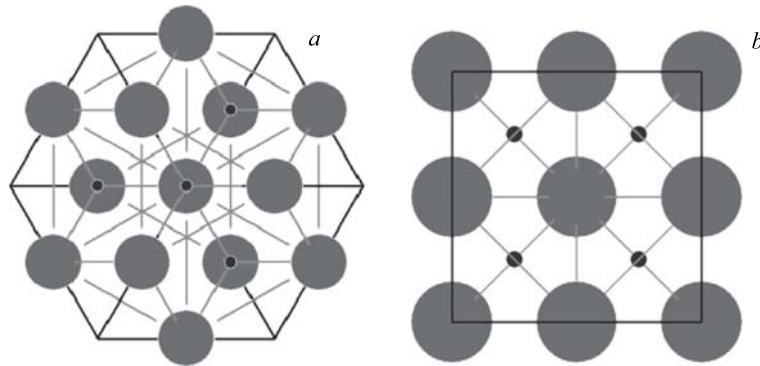


Fig. 5. TiD_2 lattice: *a*) [111] direction; *b*) [100] direction. Small black circles are positions of deuterium atoms, and large grey circles are positions of titanium atoms

is below the above-mentioned adiabatic limit. Nevertheless, a lot of experimental screening potential values (see, for example, [42]) for nuclear reactions in solids are well above this limit. There are no adequate theoretical models that could describe both anomalously large screening potentials of hundreds of electron-volts and their behavior with increasing target temperature [20]. Note that a number of experiments yield screening potential values within the adiabatic limit in some targets and well above the adiabatic limit in others [51]. This experimental and theoretical uncertainty requires other models to be devised to explain the increase in the yield of nuclear reaction products at ultralow energies.

In 2012, it was assumed that allowance for channeling of particles incident on a solid target could help one to explain enhancement of nuclear reactions in deuterium-saturated metals [44]. As the channeling angle increases with decreasing of incident energy, more and more particles participate in nuclear reactions, passing the regions with the minimum electron density, which, in turn, leads to an increase in the yield of nuclear reaction products [44].

To determine quantitatively the contribution from the channeling to the enhancement of nuclear reactions at ultralow energies, we need information on orientation of the target lattice relative to direction of the incident accelerated particle beam, because there are orientations of crystals such that deuterium atoms are completely shadowed by metal atoms. Figure 5 shows by way of example arrangement of atoms in the face-centered cubic lattice of titanium deuteride under two orientations. As an example, under orientation 5, *a*) of the face-centered cubic lattice of titanium with the Miller index [111], incident deuterons hit target deuterons only after passing through the electron density maxima in titanium atoms. Under orientation 5, *b*) with the Miller index [100], the reverse is true: all target deuterons are in the places of possible channeling of the incident particles in the electron density minimum. This simple example indicates explicit dependence of nuclear reaction product yields on the structure of a metal deuteride target. This situation can explain the above-mentioned uncertainty about screening potential in various works. This work deals with investigation of the increase in the neutron yield from the $\text{D}(d, n)^3\text{He}$ reaction at ultralow energies due to the channeling of incident particles in titanium deuteride microcrystals with a face-centered cubic lattice like TiD_2 with orientation [100].

3.3. Method for Measuring the dd -Reaction Enhancement Factor in the Channeling Mode. According to [53], there is a channeling for fast and slow particles. Classification of

particles as fast and slow is dictated by energy E [52]:

$$E_c = 2Z_1Z_2e^2d/a_2, \quad (19)$$

here Z_1 is the charge of the incident particle; Z_2 is the charge of the target nucleus; e is the electron charge; d is the spacing between the atoms in the chain, in our case, it is the lattice period, $a = a_0 \cdot 0.8853 Z_2^{-1/3}$, where a_0 is the Bohr radius.

When $E \geq E_c$, particles are considered to be fast, and the channeling angle ψ is determined by the relation [53]:

$$\psi < \psi_1 = \sqrt{\frac{E_1}{E}}; \quad E_1 = 2Z_1Z_2e^2/d, \quad (20)$$

when $E \leq E_c$, particles are considered to be slow, and the expression for the channeling angle [53]:

$$\psi < \psi_2 = \sqrt{\frac{3}{2} \frac{a}{d}} \psi_1 \quad (21)$$

reflexes its weaker dependence on energy. For titanium deuteride $d = 0.442$ nm, and accordingly the threshold energy is $E_c \approx 100$ keV. Therefore, we will further speak about channeling angles determined by relation (21).

The total yield of the *dd* neutrons from the dx layer due to the channeling effect is determined as

$$dN = InP\sigma(E_{\text{ch}}(x)) dx + In(1 - P)\sigma(E_{\text{unch}}(x)) dx + I \frac{s_{\text{rest}}}{s} n_{\text{rest}} P\sigma(E_{\text{unch}}(x)) dx, \quad (22)$$

where I is the deuteron flux hitting the deuterium target from deuterides of metal; P is the angular fraction of deuterons for which the channeling conditions are fulfilled; n_{rest} is the local density of target deuterons for particles incident at small angles on a target ‘‘column’’ with no deuterons at all, i.e., for normally incident particles we have $n_{\text{rest}} = 0$; n is by definition the density of deuterons in the target average over the layer dx ; ‘‘ch’’ and ‘‘unch’’ are the subscripts for energies of channeling and nonchanneling particles at the depth x used to discriminate between the stopping powers of particles in the channel and outside the channel; s is the total area of the target surface hit by the deuteron flux; s_{ch} is the area of channels in which channeling is possible; s_{rest} is the target area without channels, i.e., $s_{\text{ch}} + s_{\text{rest}} = s$; $\sigma(E_{\text{ch}}(x))$, $\sigma(E_{\text{unch}}(x))$ are the cross sections of the studied nuclear reaction undergoing in the channels and outside at the energy of channeling and nonchanneling particles at the depth x equal to E .

Using (21), we obtain an estimate of the incident deuteron part with the energies of 7–12 keV: $(s_{\text{rest}}/s) < (1/6)$. It is evident from the angular distributions of incident deuterons that the maximum P at the lowest deuteron energy is no larger than $(1-P)$. Since $n_{\text{rest}}/n \approx s_{\text{rest}}/s$, the third term is no larger than 3% of the second term. The last term in (21) is therefore set to zero within the model under consideration.

Considering the aforesaid, the neutron yield per unit time from an infinitely thick target is written as

$$N = IP \int_0^{\infty} n\sigma(E_{\text{ch}}(x)) dx + I(1 - P) \int_0^{\infty} n\sigma(E_{\text{unch}}(x)) dx. \quad (23)$$

This expression does not involve such quantities as the local density of deuterons in the target and the area of channels. The first term in (23) describes the contribution from the channeling particles and the second term describes the contribution from the particles moving outside the channel.

As is pointed out above, channeling particles move in the region of lower electron density. This agrees with the experimental observation that the stopping power of the fast channeling particles is about half the crystal-average one [52]. Therefore, nonchanneling particles that move through the oriented crystal at small angles pass through the region where the electron density is higher than the density average over the crystal. Nevertheless, the stopping power of slow particles in the crystal is actually not known. Within the model in question, we used the simplest dependence $(dE_{\text{ch}}/dx) = \beta^{-1}(dE/dx)$ and $(dE_{\text{unch}}/dx) = \gamma^{-1}(dE/dx)$, where (dE/dx) is the specific stopping power for particles moving in an amorphous medium. The parameters β and γ are determined from the experiment. Thus, we have a two-parameter model for the yield of nuclear reaction products from the crystalline medium

$$N = (\beta P + \gamma(1 - P))I \int_0^{\infty} n\sigma(E(x)) dx. \quad (24)$$

It follows that the parameter β should be larger than 1 and γ no larger than 1. Calculation of integrals in (24) involves specific energy losses suffered by particles moving in an amorphous medium, which are determined using the SRIM code [53].

If the stopping power for the target does not differ from that for the amorphous medium, $\beta = \gamma = 1$, the factor $\beta P + \gamma(1 - P)$ in (12) becomes unity. If $\beta \neq \gamma$, there arises energy dependence of the neutron yield in addition to that determined by the integral in (24). In what follows, we will refer to reaction product yields from an amorphous target as calculated yields, and the difference between the neutron yield and the calculated yield will be determined by the enhancement factor in the channeling model

$$f_{\text{ch}}(E_0) = \beta P(E_0) + \gamma(1 - P(E_0)). \quad (25)$$

Here E_0 is the energy of the incident particles.

The angular fraction of the channeling beam particles depends on the angular distribution of the incident particles relative to the target and the angular distribution of the target crystals.

In the next subsection, we will give data on the angular distribution of incident ions and the structure of the solid target, which allow the function $P(E)$ to be calculated.

3.4. Experimental Procedure. In this experiment, we have used the same setup as in [19–21]. The detailed description of the setup is given in Sec. 2.

We measured the angular distribution of deuterons in the beam [54] in special additional experiments. The titanium deuteride coating was produced by magnetron sputtering of titanium in a gaseous medium consisting of argon and deuterium in a volume proportion of 4:1. Figure 6 shows an electron microscope image of the titanium deuteride coating applied to a single-crystal silicon backing. It is seen that the transverse size of the crystallites that make up the surface is from 30 to 40 nm. Figure 7 shows an electron microscope image of the cleavage of the titanium deuteride coating applied to a single-crystal silicon backing by magnetron sputtering. It is seen that the coating is 1520 nm thick and consists of columnar crystallites arranged parallel to one another. The crystallites first grow at a slant. At a distance

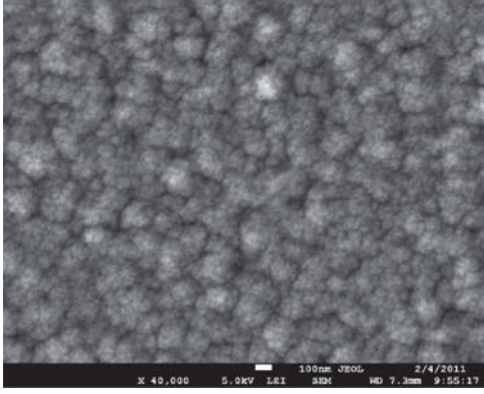


Fig. 6. Electron microscope image of the surface of the titanium deuteride coating applied to a single-crystal silicon backing by magnetron sputtering. Magnification 40,000

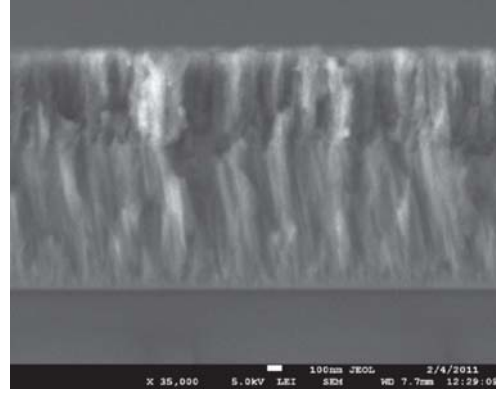


Fig. 7. Electron microscope image of a cleavage of the titanium deuteride coating applied to a single-crystal silicon backing by magnetron sputtering. Magnification 35,000

of $1 \mu\text{m}$ from the backing, the direction of their growth changes, becoming orthogonal to the backing and the target surface. Thus, we succeeded in making deuterated titanium target with all microcrystals oriented in the $[100]$ direction. Distribution deuterium concentration over the depth of the titanium deuteride layer was measured by the elastic recoil detection technique using a beam of α particles with the energy of 2.3 MeV from the Van de Graaff accelerator at the Frank Laboratory of Neutron Physics, JINR [38]. It turned out that the deuterium concentration is constant over the depth of this target, but the real stoichiometry corresponds to the formula $TiD_{1.73}$. Titanium deuteride with this stoichiometry has a crystalline structure of TiD_2 and is stable to a temperature of 300°C [55].

To obtain uniform coating, backings of stainless steel and single-crystal silicon are rotated, crossing the sputtered titanium flux many times.

3.5. Analysis and Discussion of the Results. As is mentioned above, the incident ion beam is distributed in energy with the full width at half-maximum from 14 to 16% of the average beam ion energy. The energy distribution of the beam is well described by the Gaussian function [19–21]. Designating the beam energy distribution function by $F(E)$, we write the calculated neutron yield as

$$Y_0^{\text{calc}} = N_d \varepsilon n \int_0^\infty F(E) dE \int_0^E \sigma_b(E') \left(-\frac{dE'}{dx} \right)^{-1} dE', \quad (26)$$

where N_d is the total number of deuterons that hit the target, and ε is the neutron detection efficiency.

It is convenient to change the integration order and recast (26) in the form

$$Y_0^{\text{calc}} = N_d \varepsilon n \int_0^\infty \sigma_b(E) \left(-\frac{dE}{dx} \right)^{-1} dE \int_E^\infty F(E') dE'. \quad (27)$$

The calculated neutron yield in the screening model is then written as

$$Y_{\text{scr}}^{\text{calc}} = N_d \varepsilon n \int_0^{\infty} \sigma_b(E + U_e) \left(-\frac{dE}{dx} \right)^{-1} dE \int_E^{\infty} F(E') dE', \quad (28)$$

and in the channeling model with allowance for (25) it is written as

$$Y_{\text{ch}}^{\text{calc}} = N_d \varepsilon n (\beta P(E_0) + \gamma(1 - P(E_0))) \int_0^{\infty} \sigma_b(E) \left(-\frac{dE}{dx} \right)^{-1} dE \int_E^{\infty} F(E') dE', \quad (29)$$

where E_0 is the incident ion energy average over the distribution $F(E)$, which almost coincides with the energy at the distribution peak because of smoothness of $P(E)$ on the scale of $F(E)$.

Since the S factor linearly enters the equations for neutron yields (see (6)), it cannot be explicitly extracted from (29). Therefore, we determine the constants β and γ , assuming that the astrophysical S factor for the dd reaction is known, for example, from [47],

$$S_b(E) = A_1 + EA_2, \quad (30)$$

$$A_1 = 5.3701 \cdot 10^1 \text{ keV} \cdot \text{b}, \quad A_2 = 3.3027 \cdot 10^{-1} \text{ b}.$$

Thus, comparing the calculated and experimental yields, we can find the screening potential U_e in the screening model and the parameters β and γ in the channeling model.

To see the enhancement factor of the nuclear reaction product yield from the deuterated titanium, we can use Eq. (8) or (9) for the screening model or (25) for the channeling model.

Unfortunately, this approach does not allow an explicit comparison with experiment. Therefore, we propose to compare three functions

$$f_{\text{exp}} = \frac{Y_{\text{exp}}(E_i)}{Y_0^{\text{calc}}(E_i)}, \quad f_{\text{scr}} = \frac{Y_{\text{scr}}^{\text{calc}}(U_e^0; E)}{Y_0^{\text{calc}}(E)}, \quad f_{\text{ch}} = \frac{Y_{\text{ch}}^{\text{calc}}(\beta^0, \gamma^0; E)}{Y_0^{\text{calc}}(E)}, \quad (31)$$

where $Y_{\text{exp}}(E_i)$ is the experimental neutron yield at the collision energy E_i , and U_e^0 , β^0 , and γ^0 are the screening and channeling model parameters obtained by minimizing the functional

$$\chi_{\text{ch}}^2 = \sum_{i=1}^6 \frac{(Y_{\text{ch}}^{\text{calc}}(\beta, \gamma; E_i) - Y_{\text{exp}}(E_i))^2}{(\Delta Y_{\text{exp}}(E_i))^2}, \quad \chi_{\text{scr}}^2 = \sum_{i=1}^6 \frac{(Y_{\text{scr}}^{\text{calc}}(U_e; E) - Y_{\text{exp}}(E_i))^2}{(\Delta Y_{\text{exp}}(E_i))^2}, \quad (32)$$

where $\Delta Y_{\text{exp}}(E_i)$ is the error of the experimental neutron yield.

The experiments were carried out at deuteron energies from 7 to 12 keV with a step of 1 keV. The background from cosmic radiation and natural radioactivity was continuously monitored for each energy by detecting background events in the gaps between the accelerator working pulses for a time of 10 ms equal to the duration of these pulses during which the accelerated deuteron beam is impinging on the TiD_{1.73} target. The found background was from 5 to 0.5% for the deuteron energy range $E_0 = 7\text{--}12$ keV. In addition, a special target unit was developed, which allowed a target of deuterated metal to be quickly replaced by an identical

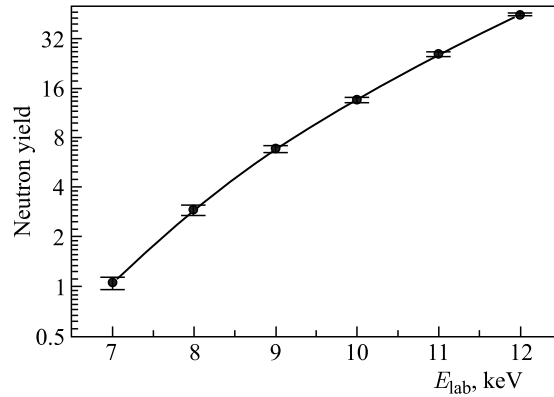


Fig. 8. Experimental yield of neutrons from the $TiD_{1.73}$ target

deuterium-free target without opening the vacuum chamber and thus to measure the neutron yield and the background under the identical conditions. The results of the neutron yield measurement from the ${}^2H(d, n){}^3He$ reaction using $TiD_{1.73}$ target with subtracted background are shown in Fig. 8. Only statistical errors, with the background taken into account, are given in Fig. 9. Fitting yielded the following values of the screening and channeling model parameters that minimize functional (30): $U_e^0 = (131 \pm 43)$ eV, $\beta^0 = 2.74 \pm 0.76$, $\gamma^0 = 0.06 \pm 0.15$.

How well the experimental data are described can be judged by Fig. 9, which shows enhancement functions (31). It is that both curves describe the experimental data well and are almost indistinguishable. The screening potential value for the dd reaction in the titanium deuteride agrees with the data of other our works [19–21, 56] and can therefore be an appropriate parameter for a comparison with the channeling model.

The channeling model parameter $\beta^0 = 2.74 \pm 0.76$, which shows how much the stopping power of a particle during channeling differs from the stopping power of a particle in an amorphous medium, does not contradict the statement [20] that the stopping power of particles

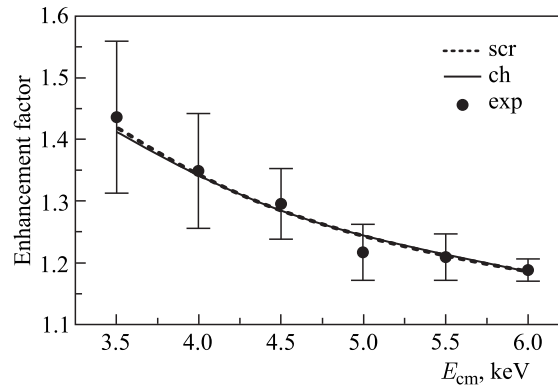


Fig. 9. Experimental and model enhancement factors; “exp” is the experimental points, “scr” is the screening model curve, and “ch” is the channeling model curve

during channeling in the region of high energies is about two times lower due to lower electron density in the channeling region. The channeling model parameter $\gamma^0 = 0.06 \pm 0.15$, which shows how much the stopping power of the particles that do not meet the channeling condition differs from that of the particle in an amorphous medium, can be treated as a statement that in the chosen energy region from 7 to 12 keV the entire contribution to the neutron yields comes from channeling particles alone. Fitting of the one-parameter channeling model at $\gamma = 0$ equally well describes the experimental data and the curves in Fig. 8.

Thus, we have come to the following conclusions:

- The channeling model does not contradict the experimental data and can explain the relative increase in the yield of nuclear reaction products at low energies.
- If the channeling model is valid, no exotic phenomena can be expected at ultralow-energy deuteron channeling in metals.
- Unlike the case in the screening model, in this model the limit in values of the enhancement factor does not tend to infinity.
- The limiting values of the increase of the yield in the channeling model are limited by the possibility for all incident particles to channel, i.e., by the value of the parameter β .
- To clarify the situation and obtain correct information on mechanisms for nuclear reactions in crystal line targets, a series of experiments with different target orientations should be conducted.
- The most reliable results can be obtained with amorphous targets or those very similar to them.
- If the channeling hypothesis is valid, no increase in the nuclear reaction product yields with decreases of deuteron collision energy should be observed in amorphous targets. Since it is technologically difficult to manufacture these targets, information on the crystal in the state of the target should be indicated for decreasing the spread of results from experiments on measurement of the neutron yield from the dd reaction.

3.6. The pd Experiment. From the standpoint of nuclear physics, it is particularly interesting to study the pd reaction in the region of ultralow proton–deuteron collision energies as a mirror reaction with respect to the reaction of radiative neutron capture by a deuteron [3,4].

As to the role of the pd reaction in nuclear astrophysics, it should be mentioned that it is an essential reaction of the Big Bang nucleosynthesis as one of the main channels for production of ^4He and it is also an important astrophysical reaction, the second step of the pp cycle governing the processes of evolution and nucleosynthesis in cold stars (in low-mass stars like our Sun, the pp cycle is one of the main ($\sim 98\%$) energy sources).

To know the pd -reaction rate in the region of ultralow energies in the order of a few keV (the position of the Gamow peak for a protostar) is necessary both for calculating characteristics of evolution of stars and protostars (the pd reaction is the beginning of the protostar development process) and for verifying stellar evolution models. Deuterium, which is burnt in this case, is the primordial deuterium that resulted from the Big Bang rather than weakly generated in the pp interaction [8].

Before the study of the pd reaction by using the Hall accelerator no theoretical and experimental information has been published about the pd reaction in deuterides (hydrides) of metals at ultralow proton–deuteron collision energies. There are only a limited number of papers devoted to the study of the pd reaction in targets of gaseous deuterium [57], heavy water D_2O [58–60], and deuterated polyethylene [34,61] (see Table 2).

Table 2. Experimental and calculated astrophysical S_{pd} factors and linear approximation parameters for $S_{pd}(E) = S_0 + S'_0 \cdot E$ (E is the center-of-mass proton–deuteron collision energy)

Reference	S_0 , eV · b	S'_0 , eV · b · keV ⁻¹	$S_{pd}(0)$, eV · b	$S_{pd}(E)$, eV · b
Viviani et al. [62]			0.185 ± 0.005	
Griffiths et al. [58]			0.25 ± 0.04	
Schmid et al. [59]	0.166 ± 0.005	0.0071 ± 0.0004	0.166 ± 0.014	
Casella et al. [57]	0.216 ± 0.006	0.0059 ± 0.0004	0.216 ± 0.010	
Bystritsky et al. [60]				0.237 ± 0.061 ($E = 8.28$ keV)
				0.277 ± 0.064 ($E = 9.49$ keV)
				0.298 ± 0.065 ($E = 10.10$ keV)

The S factor for the pd reaction depends on the proton–deuteron collision energy in a practically linear manner, as should be expected from the analysis of the s - and p -wave contributions to the cross section for the radiative proton capture by a deuteron [57–59].

Considering that the pd -reaction cross section is very small (10^{-34} – 10^{-32} cm²) in the range of ultralow proton–deuteron collision energies (a few keV), quantitative experimental determination of the contribution of the electron screening effect to the astrophysical S factor for the given reaction is problematic at the real intensities of the accelerated deuteron (proton) beams. Nevertheless, it is necessary to perform a number of experiments to determine (or estimate) the contribution of the pd -reaction enhancement in metals saturated with deuterium (hydrogen) to the astrophysical S factor. This necessity arises from the studies of the dd -reaction mechanism in some metals saturated with deuterium. Calculation in the adiabatic approximation for reactions (1a) and (1b) at deuteron collision energies near the Gamow peak indicates slight influence of the electron screening effect on the behavior of the S factor. Experiments with metallic deuterium-saturated targets, however, indicated that the electron screening potential in the dd reaction increases by one order of magnitude, which, in turn, leads to a significant increase in the astrophysical S factor in the energy range corresponding to the position of the Gamow peak [12–24, 42–46, 60]. It is not excluded that the electron screening effect can manifest itself in the pd reaction as well.

As is evident from the aforesaid and Table 2, the previous reported results of investigating the pd reaction in the region of ultralow energies on classical accelerators were ambiguous and accordingly called for further investigation of this process using radically different methods for producing higher-intensity fluxes of accelerated hydrogen ions.

A method worth noting in this respect is the one of conducting the pd experiment using the high-current pulsed Hall accelerator with the closed electron current designed by us [19–21]. We have experimentally studied for the first time the pd reaction (reaction (2)) in the proton energy ranges of 11–19 keV and 9–19 keV (laboratory system) using the targets of zirconium [26, 27] and titanium deuterides [25, 28, 29], respectively. Investigations of the pd reaction in ZrD_2 and TiD_2 allowed us to extract information about: electron screening potentials; dependences of the astrophysical factors for the pd reaction on collision proton–deuteron energy; enhancement factor of this reaction due to the electron screening effect.

Below we describe the developed experimental setup and the results of investigating of the pd reaction using solid-state deuteride targets and the pulsed Hall accelerator.

3.6.1. Experimental Method. Experimental determination of the astrophysical S factors, electron screening factors and the enhancement factors for the pd reaction in the deuterides ZrD_2 and TiD_2 in the region of astrophysical energies is based on measuring the yield of 5.5 MeV gamma quanta from reaction (2) and on using the parameterized dependence of the reaction cross sections on the proton–deuteron collision energy (7) [19–21, 26, 27, 25, 28, 29, 60].

The detailed description of the algorithm of the obtained experimental data analysis is given in Sec. 1.

3.6.2. The ZrD_2 Target. Analysis of the Experimental Data. The dependences of astrophysical S factor and effective cross section on proton–deuteron collision energy for the pd reaction occurring in zirconium deuteride at the proton energies $E_p = 11–19$ keV were measured. Figure 10 presents an example of the gamma energy spectrum obtained in one of the exposures with the ZrD_2 target at incident proton energy of 19 keV.

Figure 11 shows the dependence of the astrophysical S factor for the pd reaction on the proton–deuteron collision energy in the interval from 6.3 to 10.4 keV measured with the zirconium deuteride target in comparison with the similar dependences measured in [57, 59].

As is evident from Fig. 10, our values of the astrophysical S factor are in good agreement with the results from [57] obtained with gaseous deuterium and are greater than the results from [59] obtained with a target of heavy water (D_2O) for reasons that are still obscure.

The increasing linear dependence of the astrophysical S factor on the proton–deuteron collision energy measured in [57, 59] is confirmed within the measurement errors by the measurement in our work [26, 27]. This indicates that the pd -reaction enhancement due to the electron screening effect, if it ever exists, does not manifest itself in zirconium deuteride at the observable level. It thus follows that its influence on the intensity of the pd reaction in zirconium deuteride is much weaker than for the dd reaction. The theoretical evaluations support this conclusion. The statistical errors of measured $S_{pd}(E)$ and the limited energy interval of its measurements do not allow parameters of the linear functional dependence $S_{pd}(E) = S_0 + S'_0 \cdot E$ to be determined with a high accuracy.

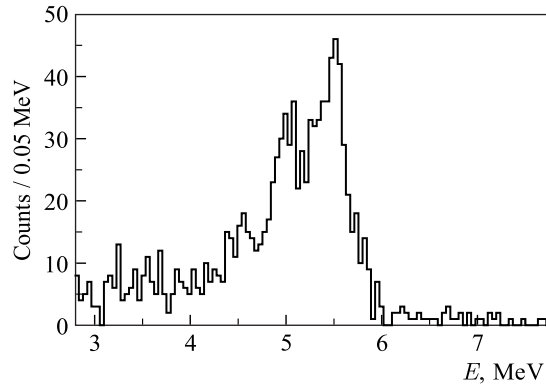


Fig. 10. Overall energy distribution of events recorded by eight NaI(Tl) detectors in exposure with the ZrD_2 target at a proton energy of 19 keV

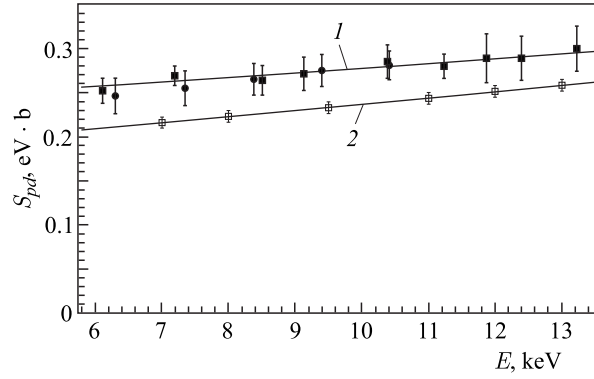


Fig. 11. Dependence of the astrophysical S factor for the pd reaction on the proton–deuteron collision energy: the filled circles are the data obtained in our experiment [26,27]; the filled squares are the experimental data obtained in [57] (experiment with the gaseous deuterium target); the empty squares are the experimental data [59] (experiment with the frozen heavy-water target); the lines 1 and 2 are the results of the experimental data fitting obtained in [57] and [59], respectively. The parameters S_0 and S'_0 of linear functional dependence $S_{pd}(E) = S_0 + S'_0 \cdot E$ have been found: $S_0 = 0.192 \pm 0.048$ eV · b, $S'_0 = 0.0087 \pm 0.0055$ eV · b · keV $^{-1}$

Figure 12 shows the dependence $\tilde{\sigma}_{pd}(E_m)$ of the effective pd -reaction cross section on the proton–deuteron collision energy E_m .

It is seen that our dependence of the pd -reaction cross section on the proton–deuteron collision energy calculated by formula $\sigma_{pd}(E) = \frac{S_{pd}(E)}{E} e^{-2\pi\eta}$ is in good agreement with

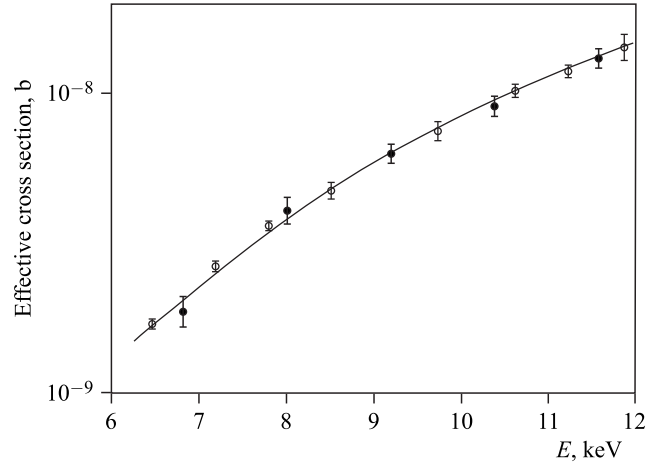


Fig. 12. Dependence of the effective pd -reaction cross section on the proton–deuteron collision energy. The filled circles are the results of our work obtained using formula (17) — $N_\gamma^{\text{exp}} = N_p n_t \varepsilon_\gamma \tilde{\sigma}_{pd}(E_m) l_{\text{eff}}(E_m) K(E_m)$, the solid curve is the calculation of the pd -reaction cross section by formula (7) — $\sigma_{pd}(E) = \frac{S_{pd}(E)}{E} e^{-2\pi\eta}$ using the corresponding measured S -factor values, and the empty circles are the effective pd -reaction cross-section values measured in [57]

the dependence of the experimentally-measured effective pd -reaction cross section on the proton–deuteron collision energy obtained using the measured gamma-ray yields and Eq. (17). Figure 12 also shows the dependence of the pd -reaction cross section on the proton–deuteron collision energy obtained using Eq. (7). It follows from this result that the expression for the gamma-ray yield from the pd reaction can be represented in a simple analytical form by introducing the quantities $\tilde{\sigma}_{pd}(E_m)$, $l_{\text{eff}}(E_m)$, and $K(E_m)$. In addition, Fig. 12 presents the experimental values of the effective pd -reaction cross section measured with the gaseous deuterium target [57].

Good agreement between the results of our work and [57] in terms of extracting information on the value of the effective pd -reaction cross section indicates that the analytical approach to determination of $\tilde{\sigma}_{pd}(E_m)$ considered by us in [30] is correct.

3.6.3. The TiD_2 Target. Analysis of the Experimental Data. The experiment included several exposures to the 9–19 keV proton beam. Figure 13 shows the depth distribution of relative atomic concentrations of titanium and deuterium in the titanium deuteride target.

The parameters of the pd reaction (2) obtained from the analysis of the experimental data are shown in Table 3.

The value of the electron screening potential U_e was obtained by fitting the measured yield of gamma quanta from reaction (2) as a function of the pd -collision energy using

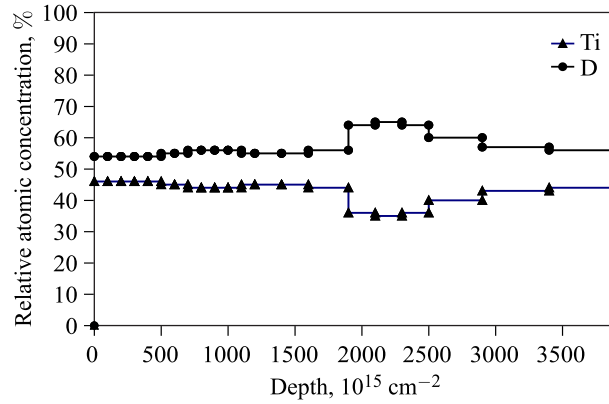


Fig. 13. Distribution of the relative atomic concentration of titanium and deuterium inside the titanium deuteride target. Black circles are the relative concentration on deuterium and black triangles are the titanium concentration

Table 3. Results of the experimental data analysis

E_p , keV	E_{col} , keV	E_m , keV	$S_{pd}^{\text{scf}}(E_{\text{col}})$, eV · b	U_e , eV	$f_{pd}^{\text{exp}}(E_{\text{col}})$	$\tilde{\sigma}_{pd}(E_m)$, nb
9	5.28	5.63	0.30 ± 0.04	242 ± 64	1.23 ± 0.14	1.20 ± 0.13
11	6.35	6.83	0.29 ± 0.03		1.19 ± 0.11	2.70 ± 0.25
13	7.41	8.03	0.29 ± 0.03		1.10 ± 0.10	4.72 ± 0.42
15	8.45	9.22	0.29 ± 0.02		1.14 ± 0.06	8.12 ± 0.44
17	9.48	10.41	0.29 ± 0.02		1.09 ± 0.06	11.58 ± 0.60
19	10.49	11.59	0.30 ± 0.02		1.07 ± 0.05	15.98 ± 0.77

expression (6), $S_{pd}^b(E)$ was replaced by $S_{pd}(E)$ from [57]. The found value of U_e is presented in Table 3. The experimental values of the enhancement factor $f_{pd}^{\text{exp}}(E)$ are determined using the expression

$$f_{pd}^{\text{exp}}(E) = \frac{N_{\gamma}^{\text{exp}}(E)}{N_{\gamma}^{\text{calc}}(E, U_e = 0)}, \quad (33)$$

where N_{γ}^{exp} is the yield of detected 5.5 MeV gamma quanta from reaction (2), $N_{\gamma}^{\text{calc}}(E, U_e = 0)$ is the calculated yield of gamma quanta from reaction (2), according to (6) on the assumption that $U_e = 0$.

Figure 14 shows the values of the enhancement factor f_{pd}^{exp} for the pd reaction as a function of the average proton–deuteron collision energy E_{col} in the proton energy range of 9–19 keV calculated by (33).

The solid line shows the result of approximating the measured dependence $f_{pd}^{\text{exp}}(E)$ by the function f_{pd}^{theor} of the form:

$$f_{pd}^{\text{theor}}(E) = \frac{N_{\gamma}^{\text{fit}}(E)}{N_{\gamma}^{\text{calc}}(E, U_e = 0)}, \quad (34)$$

where $N_{\gamma}^{\text{fit}}(E)$ is the function describing the measured dependence of the gamma quantum yield from reaction (2) on the proton–deuteron collision energy E_{col} . As is evident from Fig. 14, the experimental value of the enhancement factor is in good agreement with its values calculated by (34). This fact indicates observable manifestation of the pd -reaction enhancement due to electron screening of the interacting protons and deuterons in the TiD_2 target in the ultralow collision energy range $E_{\text{col}} = 5.3\text{--}10.5$ keV. Figure 15 shows the dependence of the astrophysical S factor $S_{pd}^{\text{scr}}(E_{\text{col}})$ in the pd reaction on the proton–deuteron collision energy E_{col} in the energy interval from 5.3 to 10.5 keV measured with the TiD_2 target.

The experimental values of the S factor in the pd reaction in the considered energy region of a pd collision were obtained using formulae (6)–(8). The uncertainties of the obtained $S_{pd}^{\text{scr}}(E_{\text{col}})$ values were calculated as a superposition of the errors in measurement of the gamma quantum yield from (6), the number and energy dependence of the incident protons, the depth distribution of the deuteron concentration in the target, and the errors in

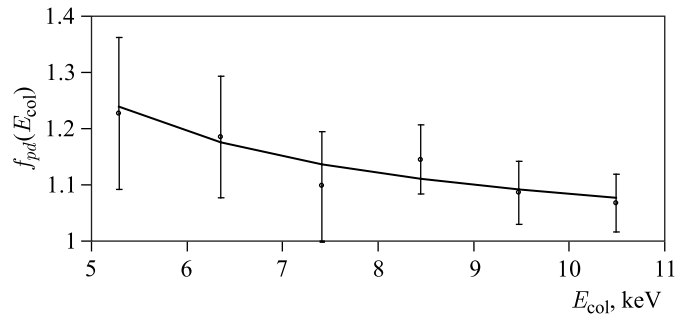


Fig. 14. Dependence of the enhancement factor f_{pd}^{exp} for the pd reaction on the average proton–deuteron collision energy E_{col} . Solid line is the result of approximating the measured dependence $f_{pd}^{\text{exp}}(E_{\text{col}})$ by expression (33)

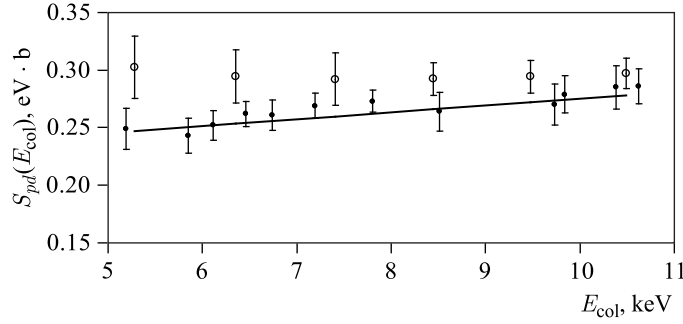


Fig. 15. Dependence of the astrophysical S factor $S_{pd}^{scr}(E_{col})$ in the pd reaction on the proton–deuteron collision energy E_{col} . Empty circles are the results of this work, filled circles are those from [57]; the solid line is the result of approximating the data from [57] by the expression $S_{pd}(E_{col}) = 0.216 + 0.0059E_{col}$

the calculation of the gamma quantum detection efficiency and the specific ionization losses of proton energy in TiD_2 in the range of ultralow collision energies.

The values of the electron screening potential U_e obtained by our team noticeably exceed the respective values of the dd reaction occurring in the analogous target and in the identical deuterium collision energy region [14, 19–21]. The result is quite unexpected because theoretical estimations practically exclude observable manifestation of the electron screening effect in this proton–deuteron collision energy range. The nature of this noticeably high effect is yet to be understood. It is not clear either why the electron screening potential for the pd reaction is more than two times as high as that for the dd reaction in the same astrophysical energy region and in the target of the same material. There is an important point related to the behavior of the dependence of the astrophysical S factor for the pd reaction on the particle energy collision in the entrance channel that is worth mentioning.

A sort of constancy shown by the function $S_{pd}^{scr}(E_{col})$ in the proton–deuteron collision energy range is, in our opinion, due to the fact that the decrease in the S factor with decreasing collision energy is compensated by the screening effect.

There is another noteworthy result, which has not been explained till now. It is the experimentally-observed enhancement of the pd reaction at ultralow collision energies in the titanium deuteride target and its absence in the Zr_2D target [26, 27].

Figure 12 shows the dependence of the measured effective cross section for the pd reaction $\tilde{\sigma}_{pd}(E_m)$ on the proton–deuteron collision energy E_m (E_m is the proton–deuteron collision energy at the maximum of the function $P(E)$). The values of $\tilde{\sigma}_{pd}(E_m)$ were determined from (17) using the experimentally-measured yield of gamma quanta from the pd reaction, calculated values of effective proton range in the target $l_{eff}(E_m)$, and the value of $K(E_m)$. The experimentally-obtained values of the effective cross section $\tilde{\sigma}_{pd}(E_m)$ are given in Table 3. In Fig. 12, cross sections for the pd reaction that are measured in [57] and correspond to particular values of the effective proton–deuteron collision energy E_m under the conditions of the given experiment are also shown for comparison. As seen in Fig. 12, the calculated dependence $\tilde{\sigma}_{pd}(E_m)$ corresponding to the conditions of the experiment [57] lies a little lower than the dependence $\tilde{\sigma}_{pd}(E_m)$ measured experimentally by us. The discrepancy between these dependences supports the existence of the electron screening effect of interacting protons and

deuterons, which results in an increase in the pd -reaction cross section as compared with the interaction of “bare” protons and deuterons (see Eqs. (8) and (9)).

To conclude, the experimental data obtained by our team from studying the pd reaction in the ultralow energy region indicate that:

- the phenomenon of electron screening in the pd reaction in titanium deuteride is experimentally observed for the first time at a high confidence level;
- no electron screening effect is found in the pd reaction occurring in zirconium deuteride, heavy water D_2O , and polyethylene deuteride;
- to explain the nature of the existing differences between the mechanisms of the pd reaction in various substances, it is necessary to conduct further research in a wider proton-deuteron collision energy range using targets of various materials: deuterated metals from various groups and periods in the table of chemical elements, semiconductors with different types of conductivity, and insulators.

Acknowledgements. The authors are grateful to A.P. Kobzev for performing measurements of atomic concentrations of deuterium and titanium in the target of titanium deuteride, I. A. Chepurchenko for maintaining the continuous operation of the Van de Graaff accelerator, and E. I. Andreev for the assistance in the preparation of the manuscript.

The work was supported by the Russian Foundation for Basic Research, project No.12-02-00086-a, the grant of the Plenipotentiary of Poland at JINR, Ministry of Education and Science of the Russian Federation, project No.2.1704.211 of the state task on research “Science”, in part by the Ministry of Education and Science of the Republic of Kazakhstan, grant No. 2023/GF3, and the grant of the Plenipotentiary of Slovakia at JINR.

REFERENCES

1. Friar J. L. // Proc. of the Intern. Conf. on the Theory of Few-Body and Quark-Hadronic System. Dubna, 1987. P. 70.
2. Chulick G. S. *et al.* Extended Parameterization of Nuclear-Reaction Cross Sections for Few-Nucleon Nuclei // Nucl. Phys. A. 1993. V. 551. P. 255.
3. Torre J., Goulard B. Mesonic Exchange Currents and Radiative Thermal Neutron Capture by the Deuteron // Phys. Rev. C. 1983. V. 28. P. 529.
4. Friar J. L. *et al.* Nuclear Transition Rates in μ -Catalyzed $p-d$ Fusion // Phys. Rev. Lett. 1991. V. 66. P. 1827.
5. Kharchenko V. F., Navrotsky M. A., Katerinchuk P. A. Effects of the Coulomb Interaction in Proton-Deuteron Scattering and Radiative Capture at Zero Energy // Yad. Fiz. 1992. V. 55. P. 86.
6. Bahcall J. N., Pinsonneault M. H. Standard Solar Models, with and without Helium Diffusion, and the Solar Neutrino Problem // Rev. Mod. Phys. 1992. V. 64. P. 885.
7. Belyaev V. B. *et al.* New Proposals for the Investigation of Strong Interaction of Light Nuclei at Super-Low Energies // Nucleonika. 1995. V. 40. P. 85.
8. Rolfs C., Rodney W. S. Cauldrons in the Cosmos. Chicago: Univ. of Chicago Press, 1988.
9. Assenbaum H. J., Langanke K., Rolfs C. Effects of Electron Screening of Low-Energy Fusion Cross Sections // Z. Phys. A: At. Nucl. 1987. V. 327. P. 461.
10. Ichimaru S. Nuclear Fusion in Dense Plasmas // Rev. Mod. Phys. 1993. V. 65. P. 255.
11. Shaviv G., Shavi N. J. Is There a Dynamic Effect in the Screening of Nuclear Reactions in Stellar Plasmas? // Astrophys. J. 2000. V. 529. P. 1054.
12. Kasagi J. *et al.* Strongly-Enhanced DD Fusion Reaction in Metals Observed for keV D^+ Bombardment // J. Phys. Soc. Japan. 2002. V. 71. P. 2881.

13. *Czerski K. et al.* Experimental and Theoretical Screening Energies for the ${}^2\text{H}(d, p){}^3\text{H}$ Reaction in Metallic Environments // *Eur. Phys. J. A.* 2006. V. 27. P. 83.
14. *Raiola F. et al.* Enhanced $d(d, p)t$ Fusion Reaction in Metals // *Ibid.* P. 79, and references therein.
15. *Huke A., Czerski K., Heide P.* Measurement of the Enhanced Screening Effect of the $d+d$ Reactions in Metals // *Nucl. Instr. Meth. B.* 2007. V. 256. P. 599, and references therein.
16. *Czerski K. et al.* Measurements of Enhanced Electron Screening in $d+d$ Reactions under UHV Conditions // *J. Phys. G: Nucl. Part. Phys.* 2008. V. 35. P. 014012, and references therein.
17. *Ruprecht G. et al.* Coherent Resonance Contributions in the Reactions ${}^6\text{Li}(d, \alpha){}^4\text{He}$ and ${}^{10}\text{B}(d, p){}^{11}\text{B}$ at the Sub-Coulomb Energies // *Phys. Rev. C.* 2004. V. 70. P. 025803.
18. *Huke A. et al.* Enhancement of the Deuteron-Fusion Reactions in Metals and Its Experimental Implications // *Phys. Rev. C.* 2008. V. 78. P. 015803.
19. *Bystritsky V. M. et al.* Measurement of Astrophysical S Factors and Electron Screening Potentials for $d(d, n){}^3\text{He}$ Reaction in ZrD_2 , TiD_2 , D_2O , and CD_2 Targets in the Ultralow Energy Region Using Plasma Accelerators // *Phys. At. Nucl.* 2012. V. 75. P. 53.
20. *Bystritsky V. M. et al.* Investigation of Temperature Dependence of Neutron Yield and Electron Screening Potential for the $d(d, n){}^3\text{He}$ Reaction Proceeding in Deuterides ZrD_2 and TiD_2 // *Ibid.* P. 913.
21. *Bystritsky V. M. et al.* Measurement of Astrophysical S Factors and Electron Screening Potentials for $d(d, n){}^3\text{He}$ Reaction in ZrD_2 , TiD_2 , and $\text{TaD}_{0.5}$ Targets in the Ultralow Energy Region Using Plasma Accelerator // *Nucl. Phys. A.* 2012. V. 889. P. 93.
22. *Bystritsky V. M. et al.* // *Izv. Vuzov. Fizika.* 2012. V. 55, No. 11/2. P. 11.
23. *Bystritsky V. M. et al.* // *JETP Lett.* 2014. V. 99, Iss. 9. P. 579–585 (in Russian).
24. *Bystritsky V. M. et al.* Experimental Verification of Hypothesis of dd Reaction Enhancement by Channeling of Deuterons in Titanium Deuteride at Ultralow Energies // *Nucl. Instr. Meth. A.* 2014. V. 764. P. 42–47.
25. *Bystritsky V. M. et al.* First Experimental Evidence of $\text{D}(p, \gamma){}^3\text{He}$ Reaction in Deuteride Titanium in Ultralow Collision Energy Region // *Ibid.* V. 753. P. 91–96.
26. *Bystritsky V. M. et al.* Measuring the Astrophysical S Factors and the Cross Sections of the $p(d, \gamma){}^3\text{He}$ Reaction in the Ultralow Energy Region Using a Zirconium Deuteride Target // *Phys. Part. Nucl. Lett.* 2013. V. 10, No. 7. P. 717–722.
27. *Bystritsky V. M. et al.* Study of the $d(p, \gamma){}^3\text{He}$ Reaction at Ultralow Energies Using a Zirconium Deuteride Target // *Nucl. Instr. Meth. A.* 2014. V. 737. P. 248–252.
28. *Bystritsky V. M. et al.* Experimental Observation of Electron Screening for the $\text{D}(p, \gamma){}^3\text{He}$ Nuclear Reaction in Titanium Deuteride TiD // *Phys. Part. Nucl. Lett.* 2014. V. 11, No. 4. P. 467–472.
29. *Bystritsky V. M. et al.* // *JETP.* 2014. V. 145, Iss. 6 (in Russian).
30. *Bystritsky V. M., Pen'kov F. M.* Analytic Estimates of the Product Yields for Nuclear Reaction in the Ultralow Energy Range // *Phys. At. Nucl.* 2003. V. 66. P. 77–82.
31. *Bystritsky V. M. et al.* Study of the Reactions between Light Nuclei in the Astrophysical Energy Using the Plasma Hall Accelerator // *Proc. of the XI Intern. Seminar on Electromagnetic Interactions of Nuclei (EMIN-2006)*, Inst. for Nucl. Res. RAS, Moscow, 2006.
32. *Butakov L. D. et al.* // *Bull. Russ. Acad. Sci. Phys.* 2007. V. 71. P. 1640.
33. *Bystritsky V. M. et al.* // *Eur. Phys. J. A.* 2008. V. 36. P. 151.
34. *Bystritsky V. M. et al.* // Application of Inverse Z -Pinch for Study of the pd Reaction at keV Energy Range // *Nucl. Instr. Meth. A.* 2006. V. 565. P. 864.
35. *Bystritsky V. M. et al.* // *Izv. Vuzov. Fizika.* 2012. V. 55, No. 11/2. P. 51.
36. *Bystritskii Vit. et al.* // *J. Appl. Phys.* 2004. V. 96. P. 1249.

37. Nechaev B. A. *et al.* // Proc. of the 15th Intern. Symp. on High-Current Electronics. Tomsk: Publ. House of the IAO SB RAS, 2008. P. 148.
38. Kobzev A. P. *et al.* // Vacuum. 2009. V. 83. P. S124.
39. Wei-Kan Chu, Mayer J. W., Nicolet M. A. Backscattering Spectrometry. New York; San Francisco; London: Acad. Press, 1978.
40. Yagi H. *et al.* // Japan. J. Appl. Phys. 1995. V. 34. P. L577.
41. Practical Surface Analysis by Auger and X-Ray Photoelectron Spectroscopy / Eds.: Briggs D., Seah M.P. New York: Wiley, 1983.
42. Raiola F. *et al.* // Eur. Phys. J. A. 2004. V. 19. P. 283.
43. Bonomo C. *et al.* // Nucl. Phys. A. 2003. V. 719. P. 37.
44. Czerski K. *et al.* // Nucl. Instr. Meth. B. 2002. V. 193. P. 183.
45. Czerski K. *et al.* // Europhys. Lett. 2004. V. 68. P. 363.
46. Raiola F. *et al.* Enhanced Electron Screening in $d(d,p)t$ for Deuterated Ta // Eur. Phys. J. A. 2002. V. 13. P. 377.
47. Bosch H. -S., Hale G. M. // Nuclear Fusion. 1992. V. 32. P. 611, and references therein.
48. Greife U. *et al.* // Z. Phys. A. 1995. V. 351. P. 107.
49. Salpeter E. E. // Aust. J. Phys. 1954. V. 7. P. 373.
50. Ashcroft N. W., Mermin N. D. Solid State Physics. New York: Holt, Rinehart, and Winston, 1976.
51. Yuki H. *et al.* // JETP Lett. 1998. V. 68. P. 823.
52. Lindhard J. // Mat.-Fis. Medd. Dan. Vid. Selsk. 1965. V. 34, No. 14.
53. Ziegler J. F., Biersack J. P. Computer Code SRIM. 2008. www.srim.org.
54. Nechaev B. A. *et al.* // Proc. of the 15th Intern. Symp. on High Current Electronics. Tomsk: Publ. House of the IAO SB RAS, 2008. P. 151.
55. Mueller W. M., Blackledge J. P., Libowitz G. G. Metal Hydrides. New York; London: Acad. Press, 1968.
56. Filipowicz M. *et al.* // Intern. J. Mod. Phys. E. 2012. V. 21. P. 1250089.
57. Casella C., Costantini H., Lemut A. // Nucl. Phys. A. 2002. V. 706. P. 203.
58. Griffiths G. M., Lal M., Scarfe C. D. // Can. J. Phys. 1963. V. 41. P. 724.
59. Schmid G. J. *et al.* // Phys. Rev. C. 1997. V. 56. P. 2565.
60. Bystritsky V. M. *et al.* // Nucl. Instr. Meth. A. 2008. V. 595. P. 543–548.
61. Bystritsky V. M. *et al.* // Sov. Yad. Fiz. 2005. V. 68. P. 1.
62. Viviani M., Schiavilla R., Kievsky A. Theoretical Study of the Radiative Capture Reactions ${}^2\text{H}(n, \gamma){}^3\text{H}$ and ${}^2\text{H}(p, \gamma){}^3\text{He}$ at Low Energies // Phys. Rev. C. 1996. V. 54. P. 553.

Received on June 11, 2015.